

# Electrochemical Investigation of Oxygen Intercalation into $\text{La}_2\text{CuO}_{4+\delta}$ Phases

E. Magnone,\* G. Cerisola,† M. Ferretti,\* and A. Barbucci†,<sup>1</sup>

\*INFM and Dipartimento di Chimica e Chimica Industriale, Università degli Studi di Genova, Via Dodecaneso 31, 16146 Genova, Italy; and

†Istituto di Chimica, Facoltà di Ingegneria, Università degli Studi di Genova, P. le Kennedy 1, 16129 Genova, Italy

Received November 20, 1997; in revised form April 21, 1998; accepted July 23, 1998

**In this work the electrochemical intercalation of oxygen in  $\text{La}_2\text{CuO}_4$  phases has been studied. Oxygen intercalation has been performed at different anodic potentials for fixed time in alkaline solution (1 M NaOH) at room temperature. The electrochemistry of the phenomena taking place at the oxide–solution interface has been investigated by cyclic voltammetry (CV), controlled-potential coulometry, and electrochemical impedance spectroscopy (EIS). The homogeneity of processed samples and the lattice parameters prior to and after oxygen intercalation have been verified by X-ray powder diffraction. SEM has been used to relate surface modification to the potential applied after electrochemical oxygen intercalation. The recent theories and knowledge of mechanisms of oxygen intercalation into the oxide lattice have been related to the experimental results. Oxygen intercalation seems to occur at potentials slightly lower than that of the oxygen evolution reaction (OER) and proceeds on a parallel pathway to  $\text{O}_2$  evolution at more anodic potentials.** © 1999

Academic Press

## INTRODUCTION

Perovskite oxides have long been studied because of technologically relevant chemical and physical properties such as ferromagnetism (e.g.,  $\text{La}_{0.5}\text{Sr}_{0.5}\text{MnO}_3$ ), antiferromagnetism (e.g.,  $\text{LaCrO}_3$ ), ferroelectricity (e.g.,  $\text{BaTiO}_3$ ), and superconductivity (e.g.,  $\text{BaPb}_{1-x}\text{Bi}_x\text{O}_3$ ) (1, 2). Since the discovery of the new class of high-temperature oxide ceramic superconductors by Bednorz and Muller in 1986, much work has been done to find new materials with higher critical temperatures (3).

One of the most important characteristics in determining the conductive, magnetic, and superconductive perovskite properties is the oxygen content or mixed-valent state of transition metal ions in the oxides. Thus a deep knowledge of the process which involves oxygen intercalation into the oxide is essential for the systematic design and tailoring of the material properties.

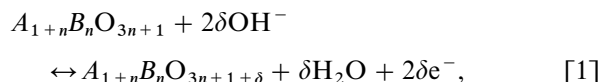
<sup>1</sup>To whom correspondence should be addressed.

Because of the relative simplicity of its structure and chemical composition,  $\text{La}_2\text{CuO}_4$  has been extensively used as a host material for oxygen insertion study.  $\text{La}_2\text{CuO}_4$  was the first layered cuprate to become a superconductor upon Ba and Sr doping, with a  $T_c$  ranging between 30 and 40 K (4), and later upon oxygen doping at high pressures, with  $T_c$  up to 34 K (5). A pressure of 3 kbar at 873 K was used to obtain proper superconducting  $\text{La}_2\text{CuO}_{4+\delta}$  with  $T_c \approx 34$  K (6).

Further research dealing with  $\text{La}_2\text{CuO}_4$  oxidation demonstrated that oxygen intercalation into oxide networks is successfully obtained by electrochemical oxidation on highly basic media at room temperature (7, 8). In this case the intercalation reaction is of particular interest because of the oxidized phase that is a bulk superconductor with an onset transition temperature of 45 K.

The advantage of this technique is related not only to a higher  $T_c$  with respect to the usual oxygenation but also to the simplified procedure. In fact, the working room temperature and simple control of oxygen input in the oxide structure make this procedure interesting in preparing highly oxidized oxides.

In the attempt to obtain oxygen oversaturation in the oxide lattice, the OER in alkaline solution has been exploited. The main principle of this technique of obtaining perovskite superconductivity stems from research on OER electrocatalysis carried out in the last decades (9–13). This process can be written in the general form

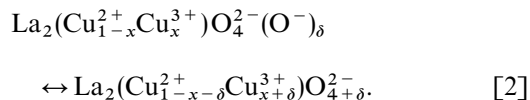


where  $A$  is a lanthanide,  $B$  is a transition metal, and  $n \geq 0$ .

Although the electrochemical methods are beginning to be widely used, the oxygen intercalation mechanism is still not entirely understood.

Casan-Pastor *et al.* (14) in their study of the thermal behavior of  $\text{La}_2\text{CuO}_{4+\delta}$  observed that a mild heating of the

electrochemically oxidized samples at 373 K causes radical changes in the structures. This was assigned to a rearrangement of the inserted oxygen atoms. They assumed the existence of  $\text{O}^-$  species at room temperature and internal redistribution of the charge carries at 373 K in accordance with the schematic model



Chronoamperometric experiments (15) and synchrotron X-ray powder diffraction studies (16) of  $\text{La}_2\text{CuO}_4$  single-crystal electrodes prepared by electrochemical oxidation show that the  $\text{O}^{2-}$  insertion is limited in diffusion length and extremely slow ( $D_{\text{O}^{2-}} \cong 10^{-16} \text{ cm}^2/\text{s}$ ) in comparison with other diffusion processes in solids (17). Moreover, the study of the electrochemical behavior of  $\text{La}_2\text{CuO}_{4+\delta}$  and  $\text{La}_{2-x}\text{Nd}_x\text{CuO}_{4+\delta}$  clearly showed that the rate-determining step of the process involves the formation of  $\text{O}^-$  species on the electrode surface whose diffusion coefficient would be  $D_{\text{O}^-} \cong 10^{-9} \text{ cm}^2/\text{s}$  (18).

From the literature, the results of studies of  $\text{La}_2\text{CuO}_4$  regarding the preparation of the oxidized phase via electrochemical oxidation demonstrate the effectiveness of this method (8, 14, 19, 20). From the electrochemical point of view, the oxygen evolution on perovskites has been the object of extensive study (12, 13, 21–23) but there is a lack of experimental works which attempt to electrochemically characterize the  $\text{La}_2\text{CuO}_4$  phase in alkaline solution.

The present study brings another view to this frame, with the help of electrochemical methods to systematically investigate the surface reactions of  $\text{La}_2\text{CuO}_4$  phases, including oxygen evolution and adsorption after oxidation in alkaline solution at 295 K. An attempt to link the electrochemistry of the  $\text{La}_2\text{CuO}_4$  oxidation phenomenon with the oxygen intercalation in the oxide bulk has also been made.

## EXPERIMENTAL

$\text{La}_2\text{CuO}_4$  samples were prepared by solid-state reaction using powders of  $\text{La}_2\text{O}_3$  (99.99%) and  $\text{CuO}$  (99.99%). The mixed powder was calcined in air at 1120 K for 15 h, re-ground, pressed into pellets ( $\varnothing = 10 \text{ mm}$ ,  $h = 3 \text{ mm}$ ), and sintered at 1300 K for 15 h. Phase recognition was performed by XRD analysis using a Philips 1710 X-ray powder diffractometer with  $\text{CuK}\alpha$  radiation.

Such prepared single-phase samples were used for the electrochemical investigation and electrochemical ageing.

The electrochemical behavior of the  $\text{La}_2\text{CuO}_4$  was investigated in sodium hydroxide aqueous solution (1 M NaOH) at room temperature. A three-compartment cell setup was used: the  $\text{La}_2\text{CuO}_4$  samples (working electrodes) were fixed in a PVC holder; a platinum net was used as a counter

electrode and a saturated calomel electrode (SCE) as reference electrode. Cyclic voltammetry (CV) was employed to study the kinetics of the electrode processes. Controlled-potential coulometry measurements were performed at various electrode potentials; pure nitrogen was used to deaerate the electrolytic solution. The oxygen dissolved in the solution was continuously checked by an  $\text{O}_2$  meter. The CV measurements and the controlled-potential coulometry were performed with a 273 G&G Princeton Research remote-controlled potentiostat–galvanostat with dedicated M 342 G&G Princeton Research software. Electrochemical impedance spectroscopy (EIS) was carried out with the same potentiostat and a 1255 Solartron frequency response analyzer. The impedance measurements were made over a frequency range of 0.05 Hz to 100 kHz (5 points per decade) with a 10-mV signal amplitude. During the CV, potential coulometry, and EIS measurements, the working electrode was kept in a controlled hydrodynamic condition with a rotating disk electrode (RDE) at 1000 rpm.

The electrochemical oxidation was carried out with the described cell setup in quiescent conditions and at different electrode potentials for a fixed time. For this purpose an AMEL Model 552 potentiostat was used.

Surface morphology was observed with an ISI SS40 scanning electron microscope (SEM).

## RESULTS AND DISCUSSION

### *Cyclic Voltammetry and Controlled-Potential Coulometry Measurements*

The oxide was subjected to anodic polarization in sodium hydroxide aqueous solution (1 M NaOH) at room temperature.

The shape of characteristic cyclic voltammograms obtained and reported by several authors (8, 14) is displayed in Fig. 1. After an initial polarization (region a), where no faradaic current is observed (the slow current increase is related to the charge equilibration at the oxide–solution interface), the  $E$ – $I$  curve shows a broad peak (region b). In this second area the current demand is mainly ascribed to oxidation of  $\text{Cu(II)}$  to  $\text{Cu(III)}$  (8, 14, 20). Afterward, the current starts to build up because of copious  $\text{O}_2$  evolution (region c). Controlled-potential measurements were then recorded, and the charge passed within 500 s is reported in Fig. 2. The trend of the charge shows that a possible transition to higher valence of Cu occurs at  $E \approx 560 \text{ mV/SCE}$ . Up to an electrode potential equal to 700 mV/SCE, the same charge can be achieved from integration of the current. After this plateau, the charge increases linearly.

The current demand recorded in the CVs has to be considered as the sum of at least two contributions: (i) the current needed to oxidize the oxide surface ( $i_{\text{Cu}^{2+}/\text{Cu}^{3+}}$ ) and (ii) the current demand for OER ( $i_{\text{OER}}$ ). The first

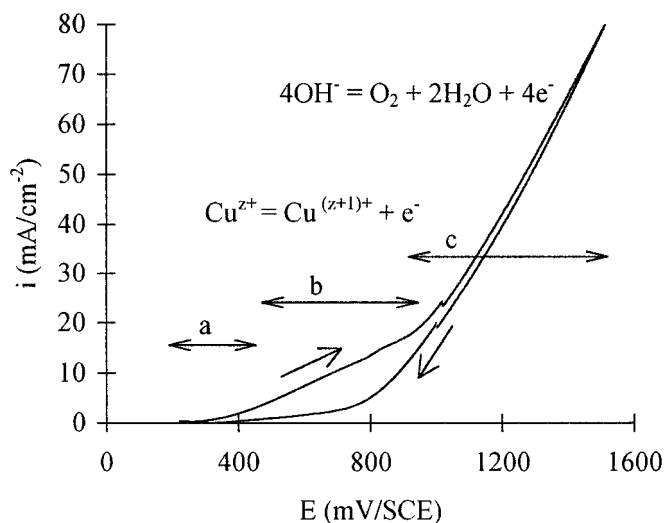


FIG. 1. Typical cyclic voltammogram of  $\text{La}_2\text{CuO}_4$  obtained in alkaline solution (5 mV/s).

contribution starts at low anodic potentials and slows down after the first oxide layer has been oxidized. The second contribution becomes significant when  $E$  enters the OER region and increases together with  $E$ . At high anodic potential, diffusion of OER reactants controls the process.

The experimental results on a  $\text{La}_2\text{CuO}_4$  sample subjected to several cyclic voltammograms show that the behavior described in Fig. 1 is mainly encountered in the first cycle; after that, a decreasing of the charge involved in the processes is displayed (Fig. 3). The trend of the charge involved for five consecutive CVs is reported in Fig. 4. Furthermore, comparison of the CVs shows a decreasing of current demand in the OER region as the CV is repeated. These two facts lead us to consider that the oxide surface undergoes an irreversible oxidation, probably through the adsorption of

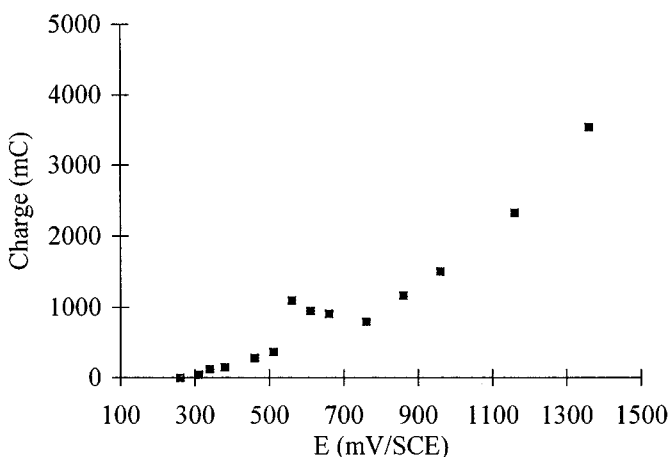


FIG. 2. Total charge passed by controlled potential coulometry.

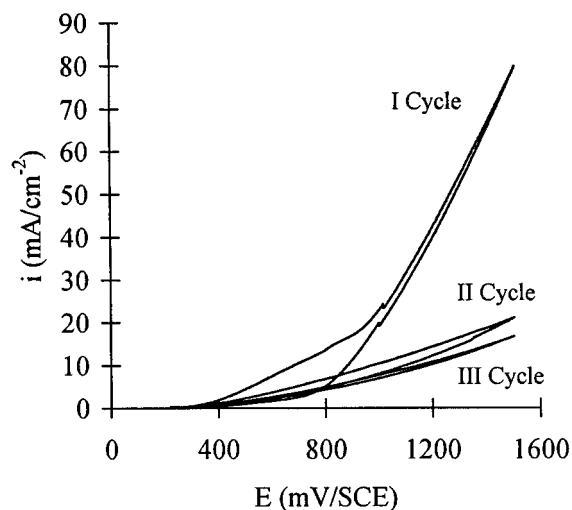


FIG. 3. Comparison of CVs consecutively performed on the same  $\text{La}_2\text{CuO}_4$  sample.

electroactive species which occupy active sites inhibiting oxygen evolution. The X-ray diffraction pattern of the oxide surface after such a treatment showed a modification of the lattice parameters with respect to the original ones. The same analysis performed after mechanical polishing of the sample surface (ca 100  $\mu\text{m}$  beneath the original surface) showed oxide lattice parameters close to the original ones.

The electrochemical oxidation was performed by polarizing the samples at two different electrode potentials for a fixed period of time (20 h): at  $E' = 600$  mV/SCE, where OER begins, and at  $E'' = 900$  mV/SCE.

The comparison of the CV obtained before and after the electrochemical oxidation performed by polarizing at  $E'$  and  $E''$  is reported in Fig. 5. It is evident that the area included in the curves changes remarkably. This difference could be ascribed to the charge associated with oxygen ion

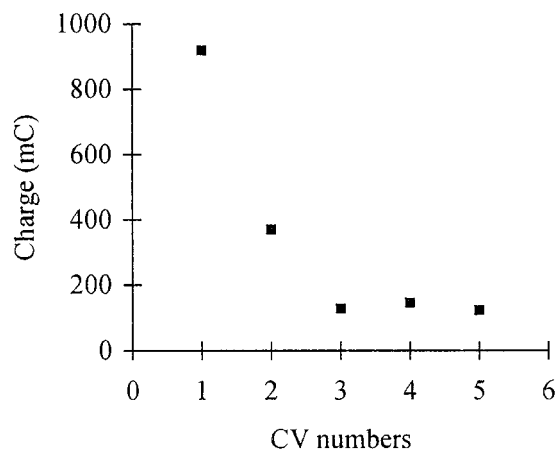
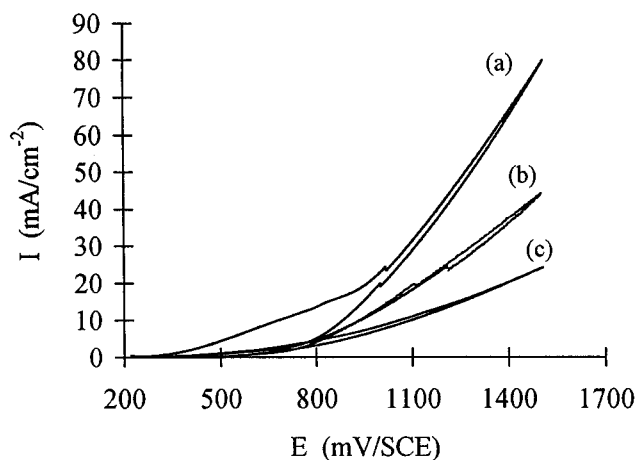


FIG. 4. Charge involved in the consecutive CVs performed on the same  $\text{La}_2\text{CuO}_4$  sample.



**FIG. 5.** Cyclic voltammogram comparison before (curve a) and after electrochemical oxidation;  $E' = 600$  mV/SCE (curve c), 900 mV/SCE (curve b).

intercalation in the  $\text{La}_2\text{CuO}_4$  lattice; it may occur more easily on the untreated electrode than on the electrochemically oxidized electrode, where the available oxygen sites are occupied. The curve obtained for the sample polarized at 900 mV/SCE shows a greater electrocatalytic activity when compared to those of the sample oxidized at 600 mV/SCE. This would be contradictory to that previously stated, also considering that in the latter curve a non-negligible charge is still involved. However, a certain increase of the electrode conductivity due to the grade of oxidation of the  $\text{La}_2\text{CuO}_4$  phase could decrease the ohmic drop in the electrode, improving, to some extent, its electrocatalytic activity.

The morphological aspects of the specimens subjected to electrochemical oxidation were then investigated by SEM (Fig. 6). The presence of characteristic pores due to sinterization and the size and boundary of the grains prior to electrochemical oxidation are displayed in Fig. 6a. Figures 6b and 6c respectively show the morphology of the specimens submitted to electrochemical oxidation at  $E = E'$  and  $E = E''$  for 20 h.

The oxidation at  $E'' = 900$  mV/SCE induces a significant modification of the surface (Fig. 6c). Here, the oxygen ion intercalation in the oxide lattice is likely to be mainly accompanied by oxygen evolution, which subjects the electrode surface to strong stress by bubble formation on the surface and porosity. Instead, the oxidation at  $E' = 600$  mV/SCE leaves the surface intact (Fig. 6b). This may be due to the decreased oxygen evolution rate. The important change in the surface morphology which occurred at the more anodic oxidation could further justify the anomalous behavior described in Fig. 5; the high surface area created by oxidation damage would support the high electrocatalytic activity.

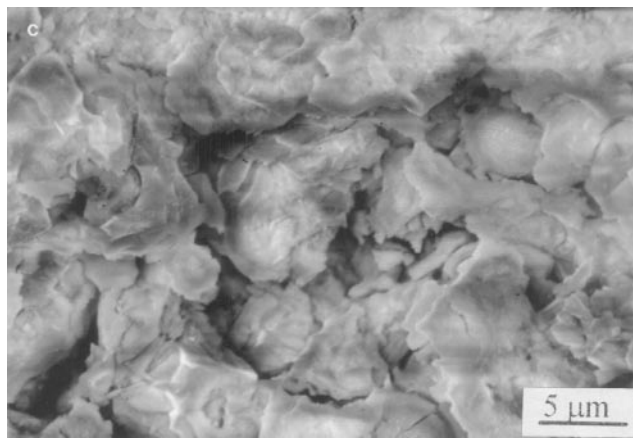
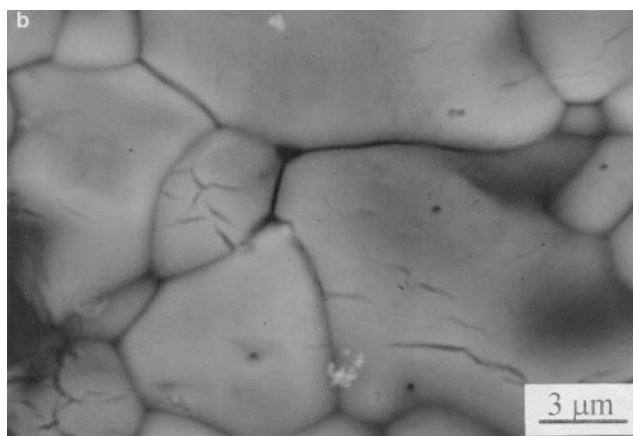
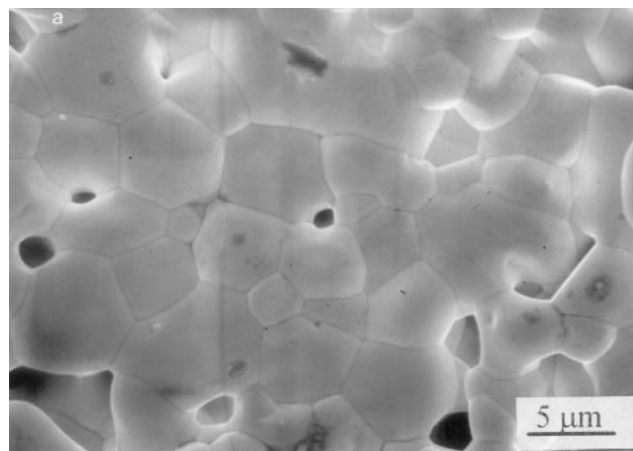


**FIG. 6.** SEM microographies of  $\text{La}_2\text{CuO}_4$  surface: starting material (a); after 20 h of electrochemical oxidation at  $E' = 600$  mV/SCE (b) and  $E'' = 900$  mV/SCE (c).

#### *XRD Characterization of $\text{La}_2\text{CuO}_{4+\delta}$ Electrodes*

The copper oxidation state in the cuprate materials can be determined directly and indirectly by several techniques (25, 26). As oxygen content in  $\text{La}_2\text{CuO}_4$  is altered, not only

does the oxidation state of the copper change, but a detectable modification of the crystal structure occurs. These structural changes are measured by the variation of the lattice parameters. Thus, the cell dimensions and its symmetry can be used as an indirect measurement of oxygen content and/or copper oxidation state (27).

Table 1 summarizes the room temperature lattice parameters  $a$ ,  $b$ , and  $c$  for the starting materials and  $\text{La}_2\text{CuO}_{4+\delta}$  as a function of  $\delta$  obtained by several research groups. It is worth noticing that the  $c$ -axis increases from 13.154 to 13.214 Å with increasing oxygen content. This  $c$  elongation is consistent with that of high-pressure oxygenated  $\text{La}_2\text{CuO}_{4+\delta}$  (28), in which oxygen is believed to be inserted in an interstitial site in  $(\text{La}_2\text{O}_2)$  layers. This interstitial oxygen is at the center of a tetrahedron formed by four La atoms.

The lattice parameters for  $\text{La}_2\text{CuO}_{4+\delta}$  are plotted against the oxygen excess ( $\delta$ ) in Fig. 7, where it is shown how  $a$  decreases linearly with increasing  $\delta$ ,  $b$  decreases with increasing  $\delta$  over the composition range  $0 \leq \delta \leq 0.05$  and subsequently increases steeply when  $\delta > 0.1$ , and  $c$  slowly increases with increasing  $\delta$  for low  $\delta$  values and stays constant for  $\delta \geq 0.1$ .

The dependence of the lattice parameters ( $a$ ,  $b$ ,  $c$ ) calculated in this work from the X-ray powder diffraction pattern versus the applied potential in the electrochemical oxidation at fixed time is plotted in Fig. 8. The lattice parameters of the starting material were  $a = 5.364$  Å,  $b = 5.412$  Å, and  $c = 13.166$  Å, whereas the orthorhombic distortion, calculated as  $f = 2(a - b)/(a + b)$ , was about 0.90%. After electrochemical oxidation at  $E' = 600$  mV/SCE, the lattice parameters were  $a = 5.345$  Å,  $b = 5.399$  Å, and  $c = 13.217$  Å and  $f \cong 1.00\%$ . The oxidation at  $E'' = 900$  mV/SCE gave  $a = 5.345$  Å,  $b = 5.425$  Å,  $c = 13.219$  Å, and  $f \cong 1.4\%$ .

**TABLE 1**  
Lattice Parameters ( $a$ ,  $b$ ,  $c$ ) of  $\text{La}_2\text{CuO}_{4+\delta}$  Phase  
as a Function of Oxygen Excess ( $\delta$ )<sup>a</sup>

$\delta$	$a$ (Å)	$b$ (Å)	$c$ (Å)	Ref.
0	5.370	5.406	13.150	36
0	5.363(5)	5.409(5)	13.17(1)	37
0	5.3572(6)	5.4011(7)	13.1542(12)	38
0.03	5.3609(5)	5.3827(5)	13.1841(11)	38
0.032	5.350(1)	5.398(3)	13.148(6)	39
0.05	5.350	5.398	13.148	40
0.09			13.203	20
0.11	5.3408(6)	5.4043(6)	13.2188(13)	38
0.138	5.341(0)	5.403(0)	13.219(1)	41
0.178	5.328	5.427	13.194	42
0.18	5.3394(15)	5.4093(15)	13.2136(68)	38
0.186	5.333(0)	5.423(0)	13.222(1)	43

<sup>a</sup> Values obtained from the literature as listed in the last column.

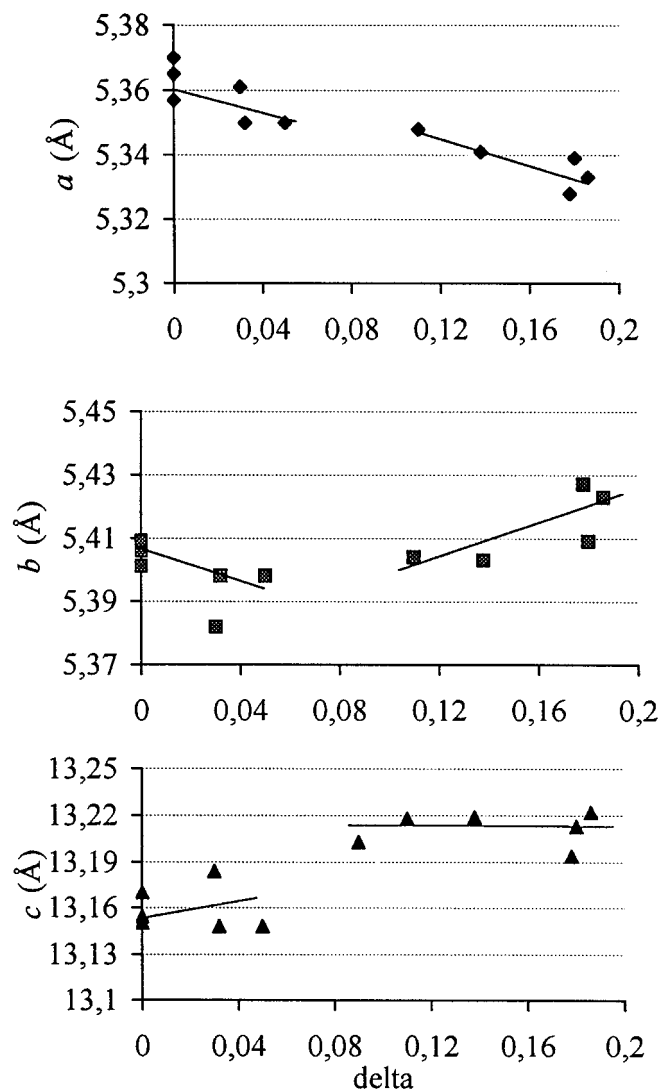


**FIG. 7.** Trend of  $\text{La}_2\text{CuO}_4$  lattice parameters ( $a$ ,  $b$ ,  $c$ ) with  $\delta$  obtained by other research works.

Comparison of these experimental results with those already reported by other authors (Fig. 7) confirms that the oxidation of  $\text{La}_2\text{CuO}_4$  has been obtained. In particular, these results show that the  $c$  parameter changes steeply at high anodic potential, the  $b$  parameter shows an initial decrease followed by an increase at higher anodic potential, and  $a$  decreases very slowly with the potentials. These trends correspond well with those already reported by Grenier *et al.* (29).

#### Electrochemical Impedance Spectroscopy Analysis

To better investigate the steps involving oxygen intercalation into the perovskite lattice, EIS measurements were performed at various electrode potentials. Typical results are shown in Fig. 9.

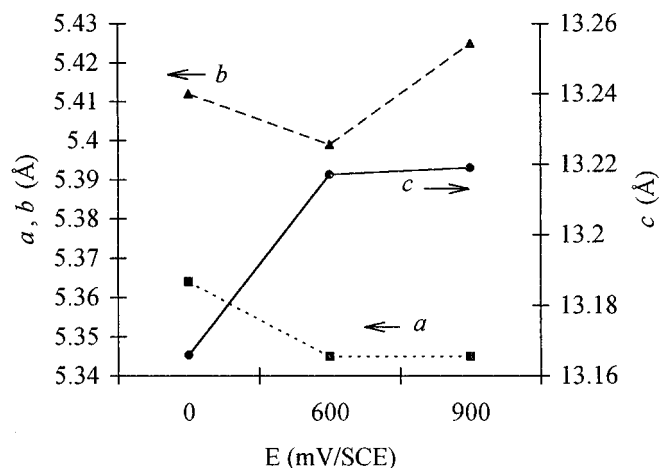


FIG. 8. Comparison of Room temperature  $\text{La}_2\text{CuO}_4$  lattice parameters  $a$  (■),  $b$  (▲),  $c$  (●) for starting materials and after the electrochemical oxidation.

The EIS results show a three-loop response typical of most ceramics (30) where the electrochemical phenomenon at the electrolyte–oxide interface and that in the oxide are displayed. In the high- and medium-frequency domains the impedance refers to the polycrystalline oxide; grain boundary electrical properties differ from those of interior grain, and thus different resistivity and space charge can be detected by EIS measurement. It is worth noticing that the high-frequency response is weakly dependent on the electrode potential applied to the system. At low frequencies ( $< 10$  Hz) the contribution to the impedance of the reactions at the oxide–electrolyte interface is shown. The frequency at which the loops show their maximum ( $f_{\text{max}}$ ) is linked to the capacitance and resistance by

$$f_{\text{max}} = 1/2\pi\tau, \quad [3]$$

where  $\tau$  (relaxation time) is

$$\tau = RC. \quad [4]$$

The high-frequency loop ( $> 10^4$  Hz) is due to the electrochemical response of the grain under the effect of the electric field applied. It appears at a higher frequency than the grain boundary loop ( $10^4$ – $10^2$  Hz) because of the dimension difference of the charged space, which is smaller with the grain boundary. In fact, the thin distribution of the charge in the grain boundary involves a higher capacitance ( $C$ ) than in the grain interior. The resistance ( $R$ ) of the grain and grain boundary is available from the intercept of the loops with the real axis of the impedance diagrams. In our case the relaxation times are sufficiently postponed in the frequency dispersion to recognize the two phenomena; however, the response is not so clear as sometimes observed in other works (30).

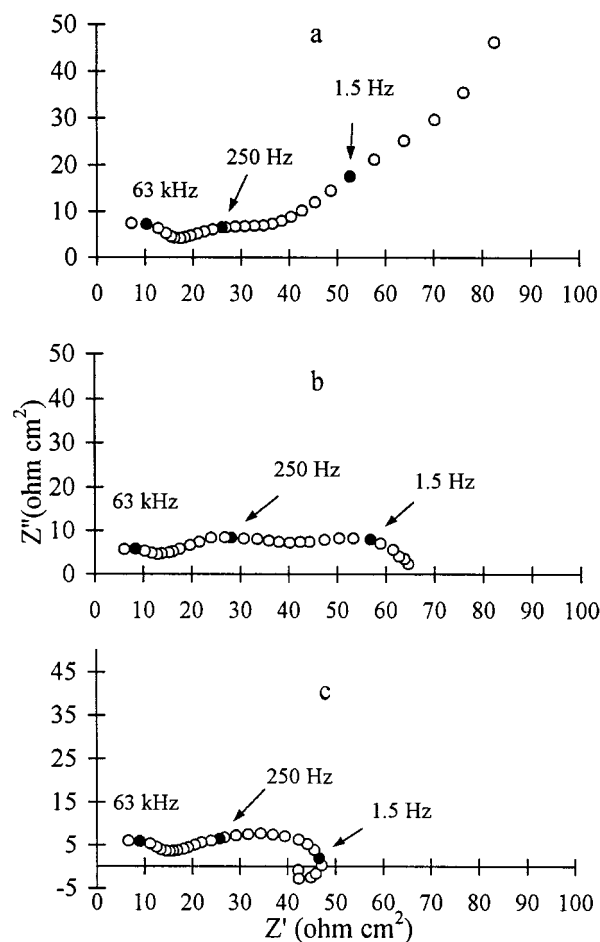


FIG. 9. Impedance spectra obtained for:  $E = E_{\text{eq}}$  (a);  $E = 600$  mV/SCE (b);  $E = 900$  mV/SCE (c).

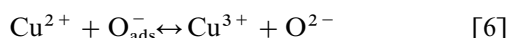
While the high- and medium-frequency dispersion of the spectra refer to the bulk properties of the  $\text{La}_2\text{CuO}_4$ , in the low-frequency domain ( $< 10$  Hz) two main situations can be singled out: (i) for  $E$  below the OER region and (ii) for  $E$  into the OER region. When  $E$  is below the OER region, a third capacitive loop is partially displayed. According to theory (31), this loop could be related to the adsorption pseudocapacitance at the oxide–solution interface; in fact, the impedance values at very low frequency ( $< 0.5$  Hz) tend toward a vertical line, indicating that the electrochemical process is limited to adsorption reaction (Fig. 9a). Another interpretation of this response at low frequencies takes account of a very weak insertion of charged species in a host lattice limited by the diffusion into the material (32).

When  $E$  approaches the OER region ( $E \geq 600$  mV/SCE), the last capacitive loop is clearly obtained (Fig. 9b), indicating the values of the charge-transfer resistance ( $R_{\text{ct}}$ , diameter of the third loop) of the oxygen evolution reaction (33). At more anodic potentials an inductive loop is partially revealed (Fig. 9c). Such impedance diagrams, in the

low-frequency domain and anodic region, are typical for the mainly charge-transfer-controlled OER taking place on a nonhomogeneous electrode surface (34). Generally, inductive loops are ascribed to an adsorption phenomenon (35).

A possible interpretation of the EIS spectra by the theoretical equivalent circuit of the two situations described is shown in Fig. 10.

The oxygen intercalation in the lattice could then be explained by the diffusion of a limited amount of oxygen temporarily bonded at the surface-solution interface. Grenier *et al.* suggested that  $O^-$  is present at the oxide surface (Eq. [5]) and can diffuse through the bulk and react, creating  $O^{2-}$  species by an electronic exchange on the metal cation (Eq. [6]) (20):



The cyclic voltammetry and controlled-potential coulometry results suggest that  $La_2CuO_4$  oxidation occurs at a potential (ca 560 mV/SCE) slightly lower than that where oxygen evolution takes place. In particular, in EIS measurements, made at electrode potentials close to 560 mV/SCE, the low-frequency loop is still open, indicating that the OER process does not take place. This agrees with a probable  $La_2CuO_4$  oxidation process whose rate is controlled by displacement of oxygen into an inner lattice-free position by

diffusion. At higher potentials this process is hindered by OER, which develops parallel and can cause destruction of the electrode surface.

## CONCLUSIONS

The characterization of the processes responsible for the  $La_2CuO_4$  oxidation has been discussed in the light of electrochemical results and with the analysis of its structural properties.

Oxygen intercalation via electrochemical oxidation in alkaline media seems to come earlier than OER, and after, to occur on a parallel pathway to oxygen evolution by the  $O^{2-}/O^-$  diffusion in the oxide bulk.

Electrochemical oxidation may result in a significant surface modification; the correct anodic overpotential has to be carefully estimated to prevent such a modification, providing, however, an acceptable oxidation kinetics.

The present scientific results highlight a possible way in which oxygen inserts itself into the oxide lattice, and although some controversy about the theory of such a process still remains, the results reported are in agreement with those of various authors.

## ACKNOWLEDGMENTS

The authors are grateful to Professor G. L. Olcese for helpful critical discussion. The financial support of the Istituto Nazionale di Fisica della Materia and of a MURST project (Leghe e composti intermetallici: stabilità, termodinamica, proprietà fisiche e reattività) is also acknowledged.

## REFERENCES

1. C. N. R. Rao and J. Gopalakrishnan, "New Directions in Solid State Chemistry." Cambridge University Press, Cambridge, 1986.
2. A. W. Sleight, J. L. Gillson, and P. E. Bierstedt, *Solid State Commun.* **17**, 27 (1975).
3. J. G. Bednorz and K. A. Muller, *Z. Phys. B* **64**, 189 (1986).
4. J. M. Tarascon, L. H. Greene, W. R. MacKinnon, G. W. Hull, and T. H. Geballe, *Science* **235**, 1373 (1987).
5. J. Beille, B. Chevalier, G. Demazeau, F. Deslandes, J. Etourneau, O. Laborde, C. Michel, P. Lejay, J. Provost, B. Raveu, A. Sulpice, J. L. Tholence, and R. Tournier, *Physica B* **146**, 307 (1987).
6. E. Schirber, B. Morosin, R. M. Merrill, P. F. Hlava, E. L. Venturini, J. F. Kwak, P. J. Nigrey, R. J. Baughman, and D. S. Ginley, *Physica C* **152**, 121 (1988).
7. A. Wattiaux, J. C. Park, J. C. Grenier, and M. Pouchard, *C. R. Acad. Sci. Paris* **310**, 1047 (1990).
8. J. C. Grenier, A. Wattiaux, N. Lagueyte, J. C. Park, E. Marguestaut, J. Etourneau, and M. Pouchard, *Physica C* **173**, 139 (1991).
9. S. Trasatti, *Electrochim. Acta* **29**, 1503 (1984).
10. A. C. C. Tseung and S. Jasem, *Electrochim. Acta* **22**, 31 (1977).
11. J. P. Hoare, "The Electrochemistry of Oxygen." Interscience, New York, 1968.
12. J. O'M. Bockris and T. Otagawa, *J. Phys. Chem.* **87**, 2960 (1983).
13. H. Tamura, H. Yoneyama, and Y. Matsumoto, in "Electrodes of Conductive Metallic Oxides" (S. Trasatti, Ed.), p. 261. Elsevier, New York, 1980.

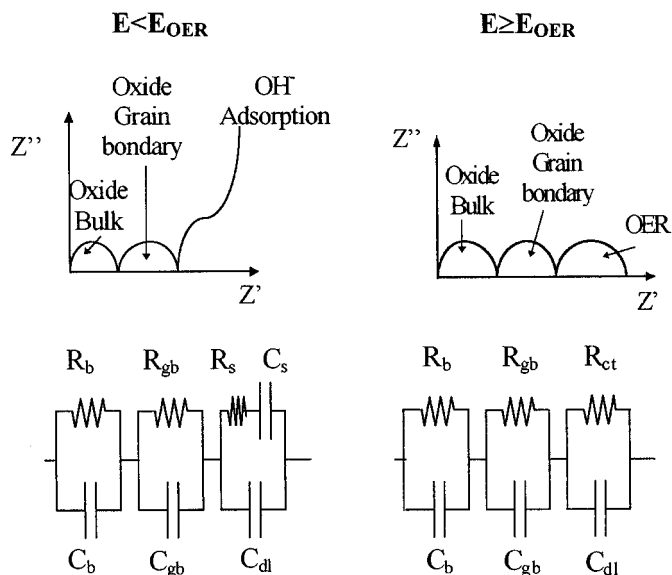


**FIG. 10.** Typical EIS spectra and theoretical equivalent circuits:  $C_b$  = bulk capacity of the grains,  $R_b$  = bulk resistivity of the grains,  $C_{gb}$  = grain boundary capacitance,  $R_{gb}$  = grain boundary resistance,  $C_{dl}$  = double layers capacitance,  $R_s$  and  $C_s$  = resistance and capacitance of adsorption phenomena,  $R_{ct}$  = charge transfer resistance of the faradaic process (OER).

14. N. Casan-Pastor, P. Gomez-Romero, A. Fuetes, J. M. Navarro, M. J. Sanchis, and S. Ondono, *Physica C* **216**, 478 (1993).
15. R. D. Sanchez, R. M. Torresi, C. Rettori, S. Oseroff, and Z. Fisk, *Electrochim. Acta* **40**, 209 (1995).
16. M. K. Crawford, R. L. Harlow, E. M. McCarron, N. Herron, W. E. Farneth, W. J. Donahue, B. A. Parkinson, and J. Schirber, *J. Phys. Chem. Solids* **56**, 1459 (1995).
17. D. M. MacArthur, *J. Electrochem. Soc.* **117**, 729 (1970).
18. J. C. Grenier, F. Arrouy, J. P. Locquet, C. Monroux, M. Pouchard, A. Villesuzanne, and A. Wattiaux, in Proceedings of "Phase Separation in Cuprate Superconductors" (K. A. Muller and E. Sigmund, Eds.), September 4–10, 1993, Cottbus, Germany, Springer-Verlag, Berlin/New York, 1993.
19. J. C. Grenier, A. Wattiaux, C. Monroux, M. Pouchard, and J. P. Locquet, *Physica C* **235–240**, 79 (1994).
20. J.-C. Grenier, A. Wattiaux, J.-P. Doumerc, P. Dordor, L. Fournes, J.-P. Chaminade, and M. Pouchard, *J. Solid State Chem.* **96**, 20 (1992).
21. J. O'M. Bockris and T. Otagawa, *J. Electrochem. Soc.* **131**, 209 (1984).
22. J. O'M. Bockris and Z. S. Minevski, *Electrochim. Acta* **39**, 1471 (1994).
23. S. Trasatti, *J. Electroanal. Chem.* **111**, 125 (1980).
24. J. M. Rosamilia and B. Miller, *Anal. Chem.* **61**, 1497 (1989).
25. W. Gruner and A. Drescher, *Fresenius Z. Anal. Chem.* **335**, 304 (1989).
26. P. Podhajecky and F. P. Dousek, *Physica C* **173**, 99 (1991).
27. R. J. Cava, B. Batlogg, C. H. Chen, E. A. Rietmann, S. M. Zahurak, and D. J. Werder, *Nature* **329**, 423 (1987).
28. "High- $T_c$  Superconductivity 1996: Ten Years after the Discovery" (E. Kaldis, E. Liarokapis, and K. A. Muller, Eds.), NATO ASI Series, Series E: Applied Sciences, Vol. 343. Kluwer Academic Publishers, Dordrecht, The Netherlands, 1997.
29. J.-C. Grenier, N. Lagueyte, A. Wattiaux, J.-P. Doumerc, P. Dordor, J. Etourneau, M. Pouchard, J. B. Goodenough, and J. S. Zhou, *Physica C* **202**, 209 (1992).
30. D. D. Macdonald, in "Transient Techniques in Electrochemistry," Section 8.5. Plenum Press, New York 1977.
31. J. R. Macdonald, in "Impedance Spectroscopy," Section 4. Wiley-Interscience, New York, 1987.
32. G. Barral, J. P. Diard, and C. Montella, *Electrochim. Acta* **29**, 239 (1984).
33. A. J. Bard and L. R. Faulkner, in "Electrochemical Methods," Section 9. John Wiley & Sons, New York, 1980.
34. H. Bachtler, W. J. Lorenz, W. Schindler, and G. Saemman-Ischenko, *J. Electrochem. Soc.* **135**, 2284 (1988).
35. R. D. Armstrong and K. Edmondson, *Electrochim. Acta* **18**, 937 (1973).
36. B. Grande, H. Mueller-Buschbaum, and M. Schweizer, *Z. Anorg. Allg. Chem.* **428**, 120 (1977).
37. J. M. Longo and P. H. Raccach, *J. Solid State Chem.* **6**, 526 (1973).
38. F. C. Chou, J. H. Cho, and D. C. Johnston, *Physica C* **197**, 303 (1992).
39. C. Chaillout, S. W. Cheong, S. W. Fisk, M. S. Lehmann, M. Marezio, B. Morosin, and J. E. Schirber, *Physica C* **158**, 183 (1989).
40. C. Chaillout, J. Chenavas, S. W. Cheong, S. W. Fisk, M. Marezio, B. Morosin, and J. E. Schirber, *Physica C* **170**, 87 (1990).
41. N. Lagueyte, F. Weill, A. Wattiaux, and J.-C. Grenier, *Eur. J. Solid State Inorg. Chem.* **30**, 859 (1993).
42. M. H. Tuilier, B. Chevalier, A. Tressaud, C. Brisson, J. L. Soubeyroux, and J. Etourneau, *Physica C* **200**, 113, (1992).
43. F. Izumi, Y.-I. Kim, E. Takayama-Muromachi, and T. Kamiyama, *Physica C* **235**, 841 (1994).